8

Indoor Channel Measurement for Wireless Communication

Hui Yu and Xi Chen
Shanghai Jiao Tong University
China

1. Introduction

In the past few years, Multiple Input Multiple Output (MIMO) system received lots of attentions, since it is capable in providing higher spectrum efficiency, as well as better transmission reliability. This improvement is brought by the multiple antennas at both sides of transmission. Since there are additional parallel sub-channels in spatial domain, system can not only increase the reliability by spatial diversity technology, but also provide higher data rate utilizing spatial multiplexing (see [1],[2], etc.). Orthogonal Frequency Division Multiplexing (OFDM) can also accommodate high data rate requirement by providing frequency multiplexing gain. To fully utilize the benefits of both technologies, the combination of the above two, MIMO-OFDM, has been employed in many wireless communication systems and protocols, such as WLAN [3] and LTE systems [4].

The introduction of MIMO-OFDM raises plenty challenges in channel estimation and measurement. Transmitted signals are reflected and scattered, resulting in a multipath spread in the received signals. Moreover, the transmitters, receivers, and reflecting or scattering objects are moving, which means that channels change rapidly over time [5]. Inter-Channel interference may also bring a destructive effect in transmission, which should be cancelled by accurate channel measurement or estimation.

As an important application of MIMO-OFDM technology, WLAN is suitable in providing high data rate service in hotspot area, such as office buildings, airports, libraries, stations, hospitals and restaurants. This means lots of MIMO-OFDM applications (such as WLAN) take place in indoor situations, where both transmitters and receivers are surrounded by mobile and static scatters. Different from outdoor scenario, there are some unique characteristics of indoor scenario. More scatters result in larger influence by multipath effect; higher density of users and overlap between different access points bring larger interference. Because of these differences in channel parameters, it is crucial to obtain a better understanding of indoor channels. Statistics such as delay spread, Doppler spread, angle spread and path loss must be estimated by detail channel measurement. This requirement rises the interests in indoor channel measurement in the past few years.

Channel measurement or estimation schemes can be divided into two major categories, blind and non-blind. Blind channel estimation method requires large data and can only exploit the statistical behavior of channel, hence, suffers a lot in fast fading channels.

On contrast, non-blind method utilizes pre-determined information in both transmitters and receivers, to measure the channel. One of the most frequently used methods is the pilot/data aided channel measurement/estimation. The method can be further divided into two sub-methods considering the resources occupied by pilots with each resource unit. In the first sub-method, pilots occupy the whole resource unit, for example, an OFDM training symbol. This type of pilot arrangement is largely used for pure purpose of channel measurement without the request of communication. In real-time communication, it is only suitable for slow channel variation and for burst type data transmission schemes. In the second sub-method, pilots only occupy part of the resource unit; the other part of the unit is allocated to data. This pilot arrangement is capable to provide real-time communication which takes place in time and frequency varying channels. However, a linear interpolation or higher order polynomial fitting should be applied to recover the whole channel, which will certainly cause some errors.

Recently, there are plenty works considering indoor channel measurement and estimations, with non-blind pilot/data aided method, each of which focuses on different aspects of the issue. In [6], authors introduced a detail design of a MIMO channel sounder. In their measurement process, they used a PN sequence as the probing signal (pilot), which occupy the whole frequency and time resources. Their measurement took place in Seoul railway station, and they used the results to illustrate the characteristics of delay and Doppler spread of indoor channel. In [7], authors provide a PC-FPGA design in solving a similar problem for WLAN system. Instead of occupying the whole channel resource, the PN sequences only insert in certain parts of the resource unit. In this way, channel measurement and transmission can be carried out simultaneously. The effect of polarized antennas has also been considered in [8]. Wireless situations include non-line-of-sight, propagation along the corridor and propagation over a metallic ceiling.

Other important applications include several scenarios such as: near-ground indoor channel aiming military or emergency usage [9], and indoor channel model for wireless sensor network and internet of things [10]. Pilot signal design is flexible. Instead of a PN sequence, other pseudolite signals are available, too. Also, the kinds of carrier signals are variable, such as an OFDM signal [7] or a GPS-based signal [11].

In addition, some rough estimations of channel parameters are provided. Most of these works based on the assumption that indoor channels follow the Ricean distribution. The most important parameter of Ricean distribution for indoor channels is the K-factor, which represents the ratio between the average power of deterministic and random components of the channel. In [12], a two-moment method of the Ricean K-factor is provided theoretically. Experimental results can be found in [13], which gives an application for the two-moment estimation of the Ricean K-factor in wideband indoor channels at 3.7 GHz. Although the Ricean distribution can only provide an unclear view of the channel, it is convenient and low-complexity estimation; thus can be applied in scenarios that require only partial channel state information.

2. Measurement schemes

As is introduced before, channel measurement schemes can be divided into two major categories, blind and non-blind. Since blind measurement and estimation is much less reliable, we only discuss non-blind pilot/data aided schemes. Two of the most frequently used schemes are discussed: measurement based on PN sequence which occupies a whole resource unit, and measurement based on OFDM pilot who occupies only part of an OFDM symbol.

2.1 Indoor channel model

The low-pass time-variant channel impulse response (CIR) is denoted as $h(\tau;t)$, which represents the response of the channel at time t due to an impulse applied at time $t-\tau$ .Then transmission can be expressed as:

$$y(t,\tau)=\sum_{n=0}^{N_{\mathrm{CIR}}-1}h(n,\tau)x(t-n,\tau)+w(t,\tau)_k \tag{1}$$

Where x is the transmit signal, and y is the transmit signal, N_{CIR} is the duration of the CIR, w is the noise sequence.

By taking the Fourier transform of $h(\tau;t)$, we can obtain the time-variant channel transfer function

$$H(f;t)=\int_{-\infty}^{+\infty}h(\tau;t)e^{-j2\pi f\tau}d\tau \tag{2}$$

On the assumption that the scattering of the channel at two different delays is uncorrelated, the autocorrelation function of $h(\tau;t)$ can be defined as:

$$\frac{1}{2}E\left[h^*(\tau_1;t)h(\tau_2;t+\Delta t)\right]=\varphi_h(\tau_1;\Delta t)\delta(\tau_1-\tau_2) \tag{3}$$

If we let $\Delta t=0$, the resulting autocorrelation function $\varphi_h(\tau)\equiv\varphi_h(\tau;0)$ is called delay power profile of the channel. The range of values of τ over which $\varphi_h(\tau)$ is essentially nonzero is called the multipath spread of the channel. Then the scattering function of the channel is defined as:

$$S(\tau;\lambda)=\int_{-\infty}^{+\infty}\varphi_h(\tau;\Delta t)e^{-j2\pi\lambda\Delta t}d\Delta t \tag{4}$$

By taking the integration of $S(\tau;\lambda)$, we obtain the Doppler power spectrum of the channel as:

$$S(\lambda)=\int_{-\infty}^{+\infty}S(\tau;\lambda)d\tau \tag{5}$$

The range of values of λ over which $S(\lambda)$ is essentially nonzero is called the Doppler spread of the channel.

Indoor channel conditions are much more complex than that of outdoor channel. There are plenty kinds of scattering figures, such as walls, tables, etc. People indoor can also act as scattering figures, and the movements of cell phones caused by this bring about worse channel conditions. As a result, angle of arrival, multipath spread and scattering factor of indoor channels are different from those of outdoor channels. Consequently, measurement schemes should be redesign carefully according to the above distingue characteristics, so as to to fulfill the needs of indoor channel measurements.

It is worth noticing that channels of phone calls made in indoor conditions are mixtures of both indoor and outdoor channels. Large scale fading, small scale fading and shadow fading should be equally considered in such channels. Each of these factors can cause a large channel capacity decrease.

2.2 Channel measurement using PN sequence

In this scheme, Pseudo-Noise (PN) Sequence is used as a probing signal. To authors' best knowledge, the most widely used binary PN sequence is the Maximum-Length-Shift-Register (MLSR) sequence. The length of MLSR sequence is $N_{\mathrm{PN}} = 2^m - 1$ bits. And one of the possible generators of this sequence is an m-stage linear feedback shift register (see [14]). As a result, MLSR sequence is periodic with period n. Within each period, there are 2^{m-1} ones and 2^{m-1} zeros.

One of the most important characteristics of the periodic PN sequence is its sharp auto-correlation. Consider an PN sequence x_k , we have :

$$\sum_{k=0}^{N_{\mathrm{PN}}-1} x_{k+m}x_k = \begin{cases} N_{\mathrm{PN}}, m = 0, \pm N_{\mathrm{PN}}, \pm 2N_{\mathrm{PN}}, \ldots \\ 0, \quad \text{Others} \end{cases} \tag{6}$$

If $N_{\mathrm{PN}} >> 1$, it is approximate that:

$$\frac{1}{N_{\mathrm{PN}}} \sum_{k=0}^{N_{\mathrm{PN}}-1} x_{k+m}x_k \approx \sum_{i=-\infty}^{+\infty} \delta_{m-iN_{\mathrm{PN}}} \tag{7}$$

We can represent the received signal y_k as the convolution of transmitted signal x_k and the CIR h_k as:

$$y_k = \sum_{n=0}^{N_{\mathrm{CIR}}-1} h_n x_{k-n} + w_k \tag{8}$$

The transmitter use PN sequence as the transmitting data x_k . If the generators of PN sequence in both transmitter and receiver are synchronous, at each time slot, receiver is aware of the transmitting PN sequence. Hence, receiver can obtain the CIR by doing a cross-correlating between y_k and x_k :

$$\begin{aligned}\hat{h}_k &= N_{\mathrm{PN}} \sum_{m=0}^{N_{\mathrm{PN}}-1} y_{m+k} x_m \\ &= \frac{1}{N_{\mathrm{PN}}} \sum_{m=0}^{N_{\mathrm{PN}}-1} \left(\sum_{n=0}^{N_{\mathrm{CIR}}-1} h_n x_{m+k-n} + w_{m+k} \right) x_m \\ &= \sum_{n=0}^{N_{\mathrm{CIR}}-1} h_n \frac{1}{N_{\mathrm{PN}}} \sum_{m=0}^{N_{\mathrm{PN}}-1} x_{m+k-n} x_m + \frac{1}{N_{\mathrm{PN}}} \sum_{k=0}^{N_{\mathrm{PN}}-1} w_{m+k} x_m \\ &= \sum_{n=0}^{N_{\mathrm{CIR}}-1} h_n \sum_{i=-\infty}^{+\infty} \delta_{k-n-iN_{\mathrm{PN}}} + \frac{1}{N_{\mathrm{PN}}} \sum_{k=0}^{N_{\mathrm{PN}}-1} w_{m+k} x_m \\ &= \sum_{i=-\infty}^{+\infty} h_{k-iN_{\mathrm{PN}}} + w'_m \end{aligned} \tag{9}$$

It can be seen that the result of cross-correlating is a summation of noise w' and the periodic extension of h_k . If $N_{\mathrm{CIR}} \le N_{\mathrm{PN}}$, a period of $\hat{h}_k$ can be used as the estimate of h_k [7].

There are two drawbacks in PN sequence measurement. First, the PN sequence takes up a great amount of time and frequency resources (most of the time, all the transmitting resources). This results in a great loss of throughput, as well as a channel mismatch caused by the delay between channel measurement and data transmission. Second, the accuracy of synchronizers in both sides should be in a high level, which raises the cost of equipments for channel measurement.

2.3 Channel measurement using OFDM pilot

Unlike measurement based on PN sequence, the pre-determined data of measurement based on OFDM pilot only occupied a relatively small percentage of time and frequency resources. Channel segments located on the pilots can be measured directly and correctly. However, other channel segments can only be estimated indirectly with some interpolations. Although the pilot-based measurement can only give an imperfect result, it provides a possibility of transmitting data and measuring channel simultaneously. This characteristic is crucial for real systems with limited feedback, such as WLAN, WiMax, LTE and LTE-A systems. There are two major problems in this scheme: how to design the pilot pattern and how to interpolate with discrete channel value on both time and frequency domain.

2.3.1 OFDM pilot pattern

OFDM pilots may be inserted in both time and frequency resources. A pilot pattern refers to the places where pilots are inserted in every OFDM symbol. An effective pilot pattern needs to be designed carefully in both frequency and time domains.

In frequency domain, according to the Nyquist sampling theorem, if we want to capture the variation of channel, the frequency space D_f between pilots should be small enough:

$$D_f \le \frac{1}{\tau_{\max} \Delta f} \tag{10}$$

where $\tau_{\max}$ represents the maximum delay of channel, and Δf denotes the frequency space between subcarriers.

If the above condition is not satisfied, the channel estimation cannot sample the accurate channel, since channel fading in frequency cannot be detected fast enough.

In time domain, spacing between pilots inserted in the same frequency is determined by the coherence time. In order to capture the variation of channel, the time space of pilots D_t must be correlated with coherence time, and must be small enough:

$$D_t \le \frac{1}{2 f_{doppler} T_f} \tag{11}$$

Where $f_{doppler}$ represents the maximum Doppler spread of channel, and T_f denotes the duration of each OFDM symbol.

However, it is worth pointing out that pilot allocation is a tradeoff of many factors in real systems. These include channel estimation accuracy, spectral efficiency of the system, wasted energy in unnecessary pilot symbols, and fading process not being sampled sufficiently. As a result, there is no optimal pilot pattern for all the channels, as fading process are varied.

Another important element of pilot pattern is the power allocation. Power is equally allocated to pilots and data symbols in regular cases. However, the accuracy of channel estimation can increase greatly with the power allocated to pilots. Considering the total power constraint, this will result in a decline of data symbols' SNR. Hence, another tradeoff between channel estimation and transmission capacity has to be evaluated.

There is a lack of pilots at the edges of OFDM symbols, which leads to a much higher error rate in such places. One simple but less effective way is to place more pilots at the edge. The drawback of this scheme is obvious: it reduces the frequency efficiency of systems. Some other scheme utilizes periodic behavior of the Fourier Transform, and establishes certain correlations between the beginning and the end of OFDM symbols. Simulations are reported to verify the effectiveness of this scheme.

2.3.2 Measurements on pilots

Channel segments locating on the pilots can be measured directly by some well-known algorithm, such as Least Square (LS) and Linear Minimum Mean Square Error (LMMSE).

Both LS and LMMSE algorithm aim to minimize a parameter: $\min\{(y_k - x_k h_k)^H (y_k - x_k h_k)\}$.

Using LS algorithm, we have:

$$\tilde{h}_{\mathrm{k}}^{\mathrm{LS}} = x_k^{-1} y_k = h_k + x_k^{-1} w_k = [\frac{y_k^1}{x_k^1}, \frac{y_k^2}{x_k^2}, \cdots, \frac{y_k^{M_k}}{x_k^{M_k}}]^T \tag{12}$$

where M_k is the length of transmit and receive signal.

Using LMMSE algorithm, we have:

$$\tilde{h}_k^{\mathrm{LMMSE}} = \mathbf{R}_{\mathrm{H}_k\mathrm{H}_k}(\mathbf{R}_{\mathrm{H}_k\mathrm{H}_k} + \frac{\beta}{SNR}\mathbf{I})^{-1}\tilde{\mathrm{H}}_k^{\mathrm{LS}} \tag{13}$$

where $\mathbf{R}_{\mathrm{H}_k\mathrm{H}_k} = E\{\mathrm{H}_k\mathrm{H}_k^*\}$ autocorrelation of channel. and $\beta = E\left\{|x_k|^2\right\}E\left\{1/|x_k|^2\right\}$.

Comparing both LS algorithm and LMMSE algorithm, we can draw the following conclusion. LS algorithm is much easier to realize and apply. LS algorithm only needs one discrete divider to estimate the channels on all the pilots. Moreover, statistical information about channel and noise are not necessary while employing LS algorithm. However, the accuracy of LS algorithm is very sensitive to the noise and synchronization errors.

On the other hand, LMMSE algorithm can be seen as a filtering on the estimation result on LS algorithm. And this filtering is based on the MMSE criteria. It can be proven that, under the same MSE conditions, estimations results of LMMSE algorithm provide a larger gain than that of LS algorithm. Drawbacks of LMMSE algorithm are also obvious. Due to the inversion operation of matrices, complexity of LMMSE algorithm is relatively high. Furthermore, LMMSE algorithm requires knowing the statistical information of channel and noise in prior, which is unrealistic in applications.

While taking the errors of estimated $\mathbf{R}_{\mathrm{H}_k\mathrm{H}_k}$ into account, the MSE and SNR gains provided by LMMSE algorithm are marginally larger than that of LS algorithm. Considering the tradeoff between complexity and performance, LS algorithm may be a better solution than LMMSE algorithm.

2.3.3 Interpolations

By applying LS or LMMSE algorithm, one can easily obtain the CIR of piloted channel segments. However, we still have no idea of channel segments not occupied with pilots. In order to obtain CIR of these segments, interpolations should be used.

The best interpolation algorithm may be 2-D Wiener filtering, since it can cancel noise as much as possible, in both frequency and time domain. However, in order to decide the weights of Wiener filtering, channel statistics must be known. Moreover, the complexity brought by matrix inversion increases gigantically with data in pilots. All of the above prevent the usage of 2-D Wiener filtering in real systems.

Some achievable interpolations include: cascade 1-D Wiener filtering, Lagrange interpolation, and transform domain interpolation.

Cascade 1-D Wiener filtering tries to realize a 2-D Wiener filtering by cascading two 1-D Wiener filtering. The complexity of cascade 1-D Wiener filtering is much less than 2-D Wiener filtering, while the performance only decreases a little bit. There two kinds of cascade 1-D Wiener filtering, in respects of interpolation order of frequency and time domain.

In frequency domain, the major interpolations include Lagrange interpolation, LMMSE interpolation, transform domain interpolation, DFT based interpolation, and low-pass filtering interpolation. In time domain, the available schemes are LMMSE interpolation, Lagrange interpolation.

2.3.3.1 Two dimensions LMMSE interpolations

Assume that the estimated channel matrix of all the piloted subcarriers is $\tilde{H}_{n',i'}, \forall\{n',i'\} \in \mathrm{P}$, where P is the set of positions of all the pilots, n' is the index in frequency domain, i' is the index in time domain. We have:

$$\tilde{H}_{n',i'} = \frac{Y_{n',i'}}{X_{n',i'}} = H_{n',i'} + \frac{N_{n',i'}}{X_{n',i'}}, \forall\{n',i'\} \in \mathrm{P} \tag{14}$$

Then, estimate the channel parameters by two dimensions interpolation filtering:

$$\hat{H}_{n,i} = \sum_{\{n',i'\} \in \Gamma_{n.i}} w_{n',i',n,i} \tilde{H}_{n',i'} \quad , \Gamma_{n.i} \subseteq \mathrm{P} \tag{15}$$

Where $w_{n',i',n,i}$ are the weights of interpolation filter, $\hat{H}_{n,i}$ is the estimated channel, $\Gamma_{n,i}$ is the number of used pilots. The number of weights in the filter is $N_{tap} = \left\| \Gamma_{n,i} \right\|$.

Applying MSE criteria, the MSE $J_{n,i}$ in subcarrier (n,i) is:

$$\begin{aligned} \varepsilon_{n,i} &= H_{n,i} - \hat{H}_{n,i} \\ J_{n,i} &= E\{\left|\varepsilon_{n,i}\right|^2\} \end{aligned} \tag{16}$$

A filter following the MMSE criteria is a two dimensions Wiener filter. According to the orthogonality of such a filter, we have:

$$E\left\{\varepsilon_{n,i} \tilde{H}^*_{n'',i''}\right\} = 0, \forall\{n'',i''\} \in \Gamma_{n,i} \tag{17}$$

Where (n'',i'') represents the positions of pilots while channel estimation is conducted.

The Wiener-Hopf equation can be derived from (17), which follows:

$$E\{H_{n,i} \tilde{H}^*_{n'',i''}\} = \sum_{\{n',i'\} \in \Gamma_{n.i}} w_{n',i',n,i} E\{\tilde{H}_{n',i'} \tilde{H}^*_{n'',i''}\}, \forall\{n'',i''\} \in \Gamma_{n,i} \tag{18}$$

Define the correlation function as:

$$\theta_{n-n'',i-i''} = E\left\{H_{n,i} \tilde{H}^*_{n'',i''}\right\} \tag{19}$$

If the mean value of noise is zero, and is independent to the transmission data, the correlation can be further expressed as:

$$\theta_{n-n'',i-i''} = E\left\{H_{n,i} \tilde{H}^*_{n'',i''}\right\} \tag{20}$$

Define the right part of (18) as the autocorrelation of channels at pilots:

$$\varphi_{n'-n'',i'-i''} = E\left\{\tilde{H}_{n',i'} \tilde{H}^*_{n'',i''}\right\} \tag{21}$$

According to (14), it follows:

$$\begin{aligned}\varphi_{n'-n'',i'-i''} &= \theta_{n'-n'',i'-i''} + \frac{\sigma^2}{E\left\{\left|X_{n',i'}\right|^2\right\}}\delta_{n'-n'',i'-i''} \\ &= \theta_{n'-n'',i'-i''} + \frac{1}{SNR}\delta_{n'-n'',i'-i''}\end{aligned} \tag{22}$$

Where $E\left\{\left|X_{n',i'}\right|^2\right\}$ is the average power of pilot symbols.

Equation (22) shows that the correlation function depends on the distance between the position of channel being estimated (n,i) and the positions of pilots employed in the estimation process (n'',i''). And the autocorrelation function depends on the distances between pilots.

Substituting (20) and (21) into (18), we have:

$$\boldsymbol{\theta}_{n,i}^{\mathrm{T}} = \mathbf{w}_{n,i}^{\mathrm{T}}\boldsymbol{\Phi} \tag{23}$$

Where $\boldsymbol{\Phi}$ is the $N_{tap} \times N_{tap}$ autocorrelation matrix, $\boldsymbol{\theta}_{n,i}$ is the correlation vector with length N_{tap}, and $\mathbf{w}_{n,i}$ is the parameter vector of filter with length N_{tap}. Therefore, the parameter of the 2-D Wiener filter is:

$$\mathbf{w}_{n,i}^{\mathrm{T}} = \boldsymbol{\theta}_{n,i}^{\mathrm{T}}\boldsymbol{\Phi}^{-1} \tag{24}$$

The full estimated channel matrix can be expressed as:

$$\hat{H}_{n,i} = \mathbf{w}_{n,i}^{\mathrm{T}}\tilde{\mathrm{H}}_{n,i} \tag{25}$$

In conclusion, the design of such a filter is to decide its parameters $\mathbf{w}_{n,i}$, which can be derived by the correlation function $\theta_{n-n'',i-i''}$ and average SNR. Unfortunately, the correlation of channel cannot be achieved accurately in real systems. Hence, approximate models with typical multipath delay profile $\rho(\tau)$ and Doppler power spectrum $S_{f_D}(f_D)$ are employed.

2-D Wiener filtering is the optimal interpolation scheme in respect of MMSE; it can obtain optimal performance theoretically. However, its requirement of prior statistic knowledge of channel matrix, as well as the complexity of matrix inversion, makes it almost impossible to apply in real systems.

2.3.3.2 Interpolations in frequency domain

A 2-D interpolation can be form by a cascade of two 1-D interpolations. By appropriate designs, such a cascade can largely reduce the complexity while maintaining a good performance. The order of interpolation should be taken into consideration. We propose to interpolate firstly in frequency domain, then to conduct the time domain interpolation. The reason is that frequency-time scheme can start once the piloted OFDM symbols receive, while time-frequency scheme has to wait for the arrivals of all the symbols in one frame or

subframe before the interpolation begins. As a result, frequency-time scheme can decrease the delay of channel measurement, hence provides more effective interpolation.

Interpolations in frequency domain aim to obtain all the channel function respond (CFR) $\hat{H}_C$, according to the measured CFR $\tilde{H}_p$ in each piloted subcarrier:

$$\hat{H}_C = \mathbf{w} \bullet \tilde{H}_p \tag{26}$$

where $\mathbf{w}$ is the frequency domain interpolation matrix, and is the channel vector of piloted subcarriers obtained by (12) or (13). We have:

$$\tilde{H}_p = \mathbf{X}_{pp}^{-1} Y_p = H_p + \mathbf{X}_{pp}^{-1} N_p = H_p + \tilde{n} \tag{27}$$

2.3.3.2.1 LMMSE interpolation

Projecting equation (23) on frequency domain, we obtain the optimal interpolation parameter vector $\mathbf{w}$ as:

$$\mathbf{R}_{\tilde{H}_p \tilde{H}_p} \mathbf{w}^* = \mathbf{R}_{\tilde{H}_p H_C} \tag{28}$$

where $\mathbf{R}_{\tilde{H}_p \tilde{H}_p} = E\{\tilde{H}_p \tilde{H}_p^*\}$ represents the autocorrelation matrix of estimation channel segments with pilots $\tilde{H}_P$, $\mathbf{R}_{\tilde{H}_p H_C} = E\{\tilde{H}_P H_C^*\}$ denotes the correlation matrix of estimation channel segments with pilots $\tilde{H}_P$ and the real channel being interpolated H_C.

If $\mathbf{R}_{\tilde{H}_p \tilde{H}_p}$ is invertible, $\mathbf{w}$ can be expressed as:

$$\mathbf{w} = \mathbf{R}_{H_C \tilde{H}_p} \mathbf{R}_{\tilde{H}_p \tilde{H}_p}^{-1} \tag{29}$$

Combining (12) and (27), it follows:

$$\begin{aligned} \mathbf{R}_{\tilde{n}\tilde{n}} &= E\{\tilde{n}\tilde{n}^*\} = E\{\mathbf{X}_p^{-1} N_p \cdot N_p^* (\mathbf{X}_p^{-1})^*\} \\ &= \sigma_n^2 E\{\mathbf{X}_p^{-1} \cdot \mathbf{I} \cdot (\mathbf{X}_p^{-1})^*\} = \sigma_n^2 E\{(\mathbf{X}_p^* \mathbf{X}_p)^{-1}\} \\ &= \mathbf{I}_{N_p} E\{1 / \left|X_k^p\right|^2\} \sigma_n^2 \end{aligned} \tag{30}$$

where X_k^p is the constellation point of piloted channel, and σ_n^2 is the power of noise.

Substituting (12) into (29), we have:

$$\mathbf{w} = \mathbf{R}_{H_C H_p} (\mathbf{R}_{H_p H_p} + \mathbf{I}_{N_p} E\{1 / \left|X_k^p\right|^2\} \sigma_n^2)^{-1} \tag{31}$$

where $\mathbf{R}_{H_C H_p}$ and $\mathbf{R}_{H_p H_p}$ are the ideal correlation and autocorrelation matrices. Further representing the CFRs of channels with their CIRs, it is obvious that $H_C = \mathbf{F}_{CL} h_L$ and $H_P = \mathbf{F}_{PL} h_L$ (where h_L is the discrete CIR, $\mathbf{F}_{CL}$ and $\mathbf{F}_{PL}$ are the corresponding DFT transform matrices). This converts (31) as followed:

$$\mathbf{w} = \mathbf{F}_{\mathrm{CL}}\mathbf{R}_{\mathrm{h_L h_L}}\mathbf{F}_{\mathrm{PL}}^{*}(\mathbf{F}_{\mathrm{PL}}\mathbf{R}_{\mathrm{h_L h_L}}\mathbf{F}_{\mathrm{PL}}^{*}+\mathbf{I}_{N_{\mathrm{p}}}E\{1/\left|X_k^{\mathrm{p}}\right|^2\}\sigma_n^2)^{-1} \tag{32}$$

Applying Parseval Theorem, which certifies that the power in frequency domain equals that of time domain, we draw the following conclusion:

$$\begin{aligned}\mathbf{w} &= \mathbf{F}_{\mathrm{CL}}\bar{\mathbf{R}}_{\mathrm{h_L h_L}}\mathbf{F}_{\mathrm{PL}}^{*}(\mathbf{F}_{\mathrm{PL}}\bar{\mathbf{R}}_{\mathrm{h_L h_L}}\mathbf{F}_{\mathrm{PL}}^{*}+\mathbf{I}_{N_{\mathrm{p}}}\frac{E\{1/\left|X_k^{\mathrm{p}}\right|^2\}\sigma_n^2}{trace(\mathbf{R}_{\mathrm{h_L h_L}})})^{-1}\\ &= \mathbf{F}_{\mathrm{CL}}\bar{\mathbf{R}}_{\mathrm{h_L h_L}}\mathbf{F}_{\mathrm{PL}}^{*}(\mathbf{F}_{\mathrm{PL}}\bar{\mathbf{R}}_{\mathrm{h_L h_L}}\mathbf{F}_{\mathrm{PL}}^{*}+\mathbf{I}_{N_{\mathrm{p}}}\frac{E\{1/\left|X_k^{\mathrm{p}}\right|^2\}\sigma_n^2}{E(\mathrm{H_C^{*}H_C})})^{-1}\\ &= \mathbf{F}_{\mathrm{CL}}\bar{\mathbf{R}}_{\mathrm{h_L h_L}}\mathbf{F}_{\mathrm{PL}}^{*}(\mathbf{F}_{\mathrm{PL}}\bar{\mathbf{R}}_{\mathrm{h_L h_L}}\mathbf{F}_{\mathrm{PL}}^{*}+\mathbf{I}_{N_{\mathrm{p}}}\frac{E\{1/\left|X_k^{\mathrm{p}}\right|^2\}E\{\left|X_k^{\mathrm{p}}\right|^2\}\sigma_n^2}{E\{\left|X_k^{\mathrm{p}}\right|^2\}E(\mathrm{H_C^{*}H_C})})^{-1}\end{aligned} \tag{33}$$

In special cases where QPSK modulation and equal power allocation are adopted, the interpolation is:

$$\mathbf{w} = \mathbf{F}_{\mathrm{CL}}\bar{\mathbf{R}}_{\mathrm{h_L h_L}}\mathbf{F}_{\mathrm{PL}}^{*}(\mathbf{F}_{\mathrm{PL}}\bar{\mathbf{R}}_{\mathrm{h_L h_L}}\mathbf{F}_{\mathrm{PL}}^{*}+\mathbf{I}_{N_{\mathrm{p}}}\frac{1}{SNR})^{-1} \tag{34}$$

where $SNR = \frac{P_r}{\sigma_n^2} = \frac{E\{\left|X_k\right|^2\}E\{\mathrm{H_C^{*}H_C}\}}{\sigma_n^2} = \frac{E\{\left|X_k^{\mathrm{p}}\right|^2\}E\{\mathrm{H_C^{*}H_C}\}}{\sigma_n^2}$.

2.3.3.2.2 Lagrange interpolation

Lagrange interpolation is widely used and easy to implement. It is a group of interpolation algorithms, including linear interpolation, Gaussian interpolation, cubic interpolation, etc. Lagrange interpolation is suitable for both frequency and time domain interpolation. However, the disadvantage of Lagrange interpolation is obvious. It is unable to cancel the noise.

Linear interpolation in frequency domain utilizes each pair of adjacent piloted channel segments to obtain the channel function within them. The interpolation process follows the following equation:

$$\hat{H}(l+d) = \left(1-\frac{d}{D}\right)\tilde{H}_p(l)+\frac{d}{\mathrm{D}}\tilde{H}_p(l+D), 1 \le d \le D-1 \tag{35}$$

where D is the interval between two adjacent pilots, $\tilde{H}_P(l)$ and $\tilde{H}_P(l+D)$ are the corresponding channel estimation results.

Gaussian interpolation in frequency domain employs the measured channels of three adjacent pilots, which can be represented as followed:

$$\hat{H}(x)=\begin{cases}\tilde{H}_p(l_{j-1})\dfrac{x-l_j}{l_{j-1}-l_j}\dfrac{x-l_{j+1}}{l_{j-1}-l_{j+1}}+\tilde{H}_p(l_j)\dfrac{x-l_{j-1}}{l_j-l_{j-1}}\dfrac{x-l_{j+1}}{l_j-l_{j+1}} \\ +\tilde{H}_p(l_{j+1})\dfrac{x-l_{j-1}}{l_{j+1}-l_{j-1}}\dfrac{x-l_j}{l_{j+1}-l_j},(l_j\neq K_{\max}) \\ \tilde{H}_p(l_{j-2})\dfrac{x-l_{j-1}}{l_{j-2}-l_{j-1}}\dfrac{x-l_j}{l_{j-2}-l_j}+\tilde{H}_p(l_{j-1})\dfrac{x-l_{j-2}}{l_{j-1}-l_{j-2}}\dfrac{x-l_j}{l_{j-1}-l_j} \\ +\tilde{H}_p(l_j)\dfrac{x-l_{j-2}}{l_j-l_{j-2}}\dfrac{x-l_{j-1}}{l_j-l_{j-1}},(l_j=K_{\max})\end{cases} \tag{36}$$

Where $K_{\max}$ denotes the maximum position of pilots, $\tilde{H}_P(l_{j-1})$, $\tilde{H}_P(l_j)$, and $\tilde{H}_P(l_{j+1})$ are the channel measurement results of three used pilots, and $l_{j-1}<x<l_j$.

Cubic interpolation further increase the number of used pilots onto four. The expression for interpolation is showed as followed:

$$\begin{aligned}\hat{H}(x)&=\tilde{H}_p(l_{j-2})\frac{x-l_{j-1}}{l_{j-2}-l_{j-1}}\frac{x-l_j}{l_{j-2}-l_j}\frac{x-l_{j+1}}{l_{j-2}-l_{j+1}}+\tilde{H}_p(l_{j-1})\frac{x-l_{j-2}}{l_{j-1}-l_{j-2}}\frac{x-l_j}{l_{j-1}-l_j}\frac{x-l_{j+1}}{l_{j-1}-l_{j+1}} \\ &+\tilde{H}_p(l_j)\frac{x-l_{j-2}}{l_j-l_{j-2}}\frac{x-l_{j-1}}{l_j-l_{j-1}}\frac{x-l_{j+1}}{l_j-l_{j+1}}+\tilde{H}_p(l_{j+1})\frac{x-l_{j-2}}{l_{j+1}-l_{j-2}}\frac{x-l_{j-1}}{l_{j+1}-l_{j-1}}\frac{x-l_j}{l_{j+1}-l_j} \\ &(l_j\neq K_{\max},l_j\neq d,l_{j-1}<x<l_j)\end{aligned} \tag{37}$$

All the above schemes are simple to apply in real systems. However, they all introduce certain level of noise, and yield effect of error floor. This can be eliminated by employing a low pass filter after interpolation.

2.3.3.2.3 Transform domain interpolation

The basic idea of transform domain interpolation is to reduce the complexity by conducting interpolation in various transform domains. The most widely used kind of transform domain interpolation is based on DFT.

The fundamental principle of DFT based interpolation is: in process of signal processing, zeroizing in time domain is equivalent to interpolating in frequency domain. If a sequence of N points has $N-N_{\mathrm{p}}$ zeros in the end, its Fourier transform values at the positions of multiples of N_{p} are the same as the counterparts of Fourier transform of sequence formed by the former N_{p} points. On the other hand, the Fourier transform values not at the positions of multiples of N_{p} consist of linear combinations of the Fourier transform of truncated sequence.

After receiving the information of piloted channels, DFT based interpolation conducts IFFT of length N_{p}. Then the interpolation zeroizes the transformed sequence into a N pointed sequence. Finally, transform the sequence into frequency domain by a N points FFT.

The zeroizing can be conducted as followed:

$$\hat{h}_N(i)=\begin{cases}\tilde{h}_{N_\mathrm{P}}(i) & 0\le i<N_\mathrm{p}/2\\ 0 & N_\mathrm{p}/2\le i<N-N_\mathrm{p}/2\\ \tilde{h}_{N_\mathrm{P}}(i-(N-N_\mathrm{p})) & N-N_\mathrm{p}/2\le i\le N-1\end{cases} \tag{38}$$

Considering the influences of noise and inter-channel interference, introducing a low pass filtering before zeroizing can effective increase the accuracy of channel measurement. The block diagram of the above procedure is showed in Fig. 1.

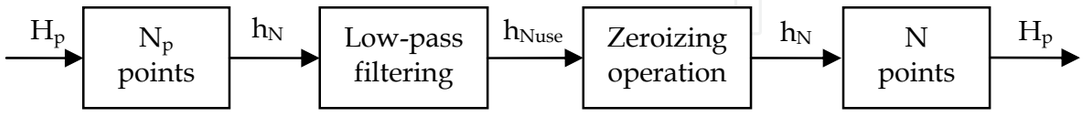

Fig. 1. DFT and low-pass filter based interpolation.

Since the most complex calculations in this kind of interpolation are FFT and IFFT, the complexity of DFT based interpolation is much lower than others. However, the performance will drop largely, if the multipath spread is not a multiple of sampling period.

2.3.3.3 Interpolations in time domain

After frequency interpolation is done, we can launch the interpolation in time domain. The interpolation can also be expressed as a interpolation matrix as followed:

$$\hat{\mathrm{H}}_{\mathrm{Ct}}=\mathbf{w}_\mathrm{t}\bullet\tilde{\mathrm{H}}_{\mathrm{pt}} \tag{39}$$

Where $\mathbf{w}_\mathrm{t}$ is the time domain interpolation matrix, $\tilde{\mathrm{H}}_{\mathrm{pt}}$ denotes the CFR of channel segments on the pilots, $\hat{\mathrm{H}}_{\mathrm{Ct}}$ represents the CFR for all the channel segments. By assuming $\tilde{\mathrm{H}}_{\mathrm{pt}}=\mathrm{H}_{\mathrm{pt}}+\tilde{\mathrm{n}}$, we consider the impact of AWGN in the interpolation.

2.3.3.3.1 LMMSE interpolation

LMMES interpolation in time domain is similar to that in frequency domain. The only difference is that we project equation (23) into time domain, so that it follows:

$$\mathbf{w}_\mathrm{t}=\mathbf{R}_{\mathrm{H_{Ct}}\tilde{\mathrm{H}}_{\mathrm{pt}}}\mathbf{R}^{-1}_{\tilde{\mathrm{H}}_{\mathrm{pt}}\tilde{\mathrm{H}}_{\mathrm{pt}}} \tag{40}$$

where $\mathbf{R}_{\tilde{\mathrm{H}}_{\mathrm{pt}}\tilde{\mathrm{H}}_{\mathrm{pt}}}=E\{\tilde{\mathrm{H}}_{\mathrm{pt}}\tilde{\mathrm{H}}^{*}_{\mathrm{pt}}\}$ represents the autocorrelation matrix of estimation channel segments with pilots $\tilde{\mathrm{H}}_{\mathrm{Pt}}$, $\mathbf{R}_{\mathrm{H_{Ct}}\tilde{\mathrm{H}}_{\mathrm{pt}}}=E\{\mathrm{H_{Ct}}\tilde{\mathrm{H}}^{*}_{\mathrm{pt}}\}$ denotes the correlation matrix of estimation channel segments with pilots $\tilde{\mathrm{H}}_{\mathrm{Pt}}$ and the real channel being interpolated $\mathrm{H_{Ct}}$.

Following the steps of derivation for frequency LMMSE interpolation, the interpolation matrix of time LMMSE interpolation can be simplified as below:

$$\mathbf{w}_\mathrm{t}=\mathbf{R}_{\mathrm{H_{Ct}H_{pt}}}(\mathbf{R}_{\mathrm{H_{pt}H_{pt}}}+\frac{\beta}{SNR}\mathbf{I}_{N_{\mathrm{pt}}})^{-1} \tag{41}$$

We consider a special case where QPSK modulation and average power allocation are used. Then the correlation between adjacent pilots i and i'' is:

$$R_{\mathrm{H_{Ct}H_{pt}}}(i,i'') = J_0(2\pi f_{D_{\max}}(i-i'')T_s') \tag{42}$$

Where $f_{D_{\max}}$ is the maximum Doppler spread, T_s' is the interval between two symbols, and $J_0(x)$ represents the first zero-order Bessel function.

However, the previous frequency interpolation and the corresponding filtering cause changes in the noise power of each subcarrier. Therefore, the signal-to-noise-ratio of each channel segment no longer equals the original value. An adjustment was proposed based on the MSE after the frequency interpolation.

Assume that channel frequency response after frequency LMMSE interpolation is:

$$\mathrm{H}_f^n = [H_0^{(n)} + \tilde{w}_0^{(n)}, \cdots, H_i^{(n)} + \tilde{w}_i^{(n)}, \cdots, H_{L-1}^{(n)} + \tilde{w}_{L-1}^{(n)}]^{\mathrm{T}} \tag{43}$$

Where L is the number of OFDM symbols in each frame, $H_i^{(n)}$ represents the channel frequency response of i$^{\text{th}}$ OFDM symbol in n$^{\text{th}}$ subcarrier, $\tilde{w}_i^{(n)}$ denotes the corresponding residual noise. Hence, variance of $\tilde{w}_i^{(n)}$ is equivalent to the MSE after interpolation.

$$MSE_{LMMSE,n} = [\mathbf{R}_{\mathrm{H_C H_C}} - \mathbf{R}_{\mathrm{H_C H_p}}(\mathbf{R}_{\mathrm{H_p H_p}} + \mathbf{I}_{N_\mathrm{p}} E\{1/\left|X_k^{\mathrm{p}}\right|^2\}\sigma_n^2)^{-1}\mathbf{R}_{\mathrm{H_C H_p}}^{\mathrm{H}}]_{nn}, n = 0,1,2,\cdots,N-1 \tag{44}$$

Where N is the number of subcarriers waiting for measured.

As a result, time domain LMMSE interpolation should be optimized according to the variance of noise. The interpolation matrix is then:

$$\mathbf{w}_{\mathrm{t}} = \mathbf{R}_{\mathrm{H_{Ct}H_{pt}}}(\mathbf{R}_{\mathrm{H_{pt}H_{pt}}} + \mathrm{diag}(\sigma_0^2, \cdots, \sigma_i^2, \cdots, \sigma_{L-1}^2))^{-1} \tag{45}$$

Where σ_i^2 represents the variance of residual noise $\tilde{w}_i^{(n)}$.

To reduce the complexity, channel segments in the same OFDM symbol can utilize their average noise variance in the interpolation, and an approximate interpolation matrix can be expressed as followed:

$$\mathbf{w}_{\mathrm{t}} = \mathbf{R}_{\mathrm{H_{Ct}H_{pt}}}(\mathbf{R}_{\mathrm{H_{pt}H_{pt}}} + \frac{1}{N}\sum_{i=0}^{N-1}\sigma_0^2(i)\mathbf{I}_L)^{-1} \tag{46}$$

2.3.3.3.2 Lagrange interpolations

Lagrange interpolations in time domain are almost the same as those in frequency domain. The only difference is channel response of piloted channel segments. One can refer to previous sections for details.

3. Applications

Here we show some useful and easily implemented examples to illustrate the indoor channel measurement. Measurement based on PN sequence, as well as OFDM pilot, will be discussed.

3.1 Channel measurement system using PN sequence

In this section, we present an example of 2x2 MIMO channel measurement, utilizing a semi-sequential scheme. This semi-sequential scheme uses parallel receivers and a switch at the transmitter (Fig. 2). When a measurement process starts, the probing signal is firstly transmitted from the 1st transmit antenna (TX1) and the receive signal is sampled from 1st and 2nd receive antennas (RX1 and RX2) simultaneously. Thus the channel from TX1 to RX1 and RX2 can be measured at the same time. Then, a similar process is used to measure the channel from TX2 to RX1 and RX2. Strictly speaking, the semi-sequential MIMO channel sounder measures Single Input Multiple Output (SIMO) channels directly. The MIMO channel is obtained by combine the two SIMO channels, on the assumption that the MIMO channel doesn't change significantly in a single round of sequential measurement.

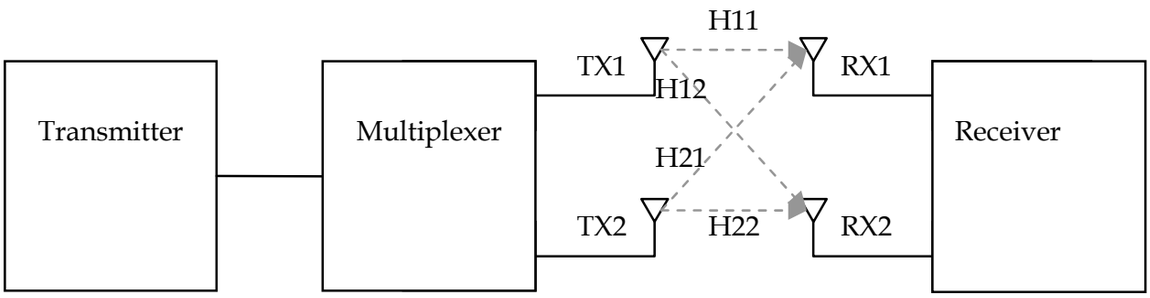

Fig. 2. Semi-sequential scheme of MIMO channel sounder [7].

Each SIMO channel can be measured by the algorithm introduced in Section 2.2 Then a combination of two SIMO channel construct the whole MIMO channel.

3.1.1 Baseband signal processing algorithm

3.1.1.1 System parameters

The link-level block diagram of the sliding correlation channel sounder for Single Input Single Output (SISO) channel is shown in Fig. 3. In the semi-sequential MIMO channel sounder (or SIMO channel sounder); there should be two parallel receivers.

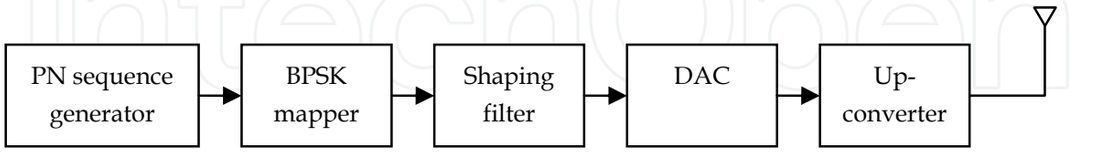

(a) Transmitter

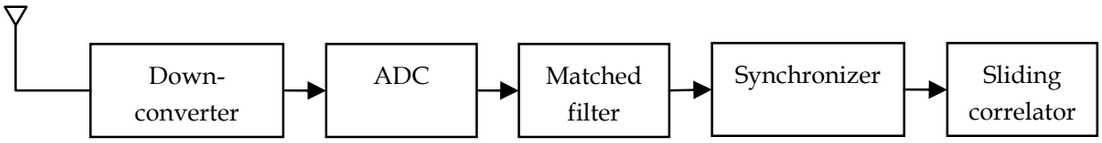

(b) Receiver

Fig. 3. Channel Sounder for SISO.

Here we only focus on the indoor wireless MIMO channel for WLAN like devices. The measurement system supports 20/40MHz bandwidth by suitable RFIC [16][17]. The system parameters of baseband are listed in Table 1.

Name	Symbol	Value
Sampling frequency	f_{s}	60MHz
Symbol rate of PN sequence	R_{symb}	20M Symbol/s
Period of PN sequence, express in units of T_{symb}	N_{PN}	127
Length of CIR, express in units of T_{symb}	N_{CIR}	127
Sampling interval	T_{s}	$1/f_{\mathrm{s}}$
Interpolated sample interval	T_{i}	$T_{\mathrm{symb}}/2$
Symbol interval of PN sequence	T_{symb}	$1/R_{\mathrm{symb}}$

Table 1. System Parameters.

3.1.1.2 Symbol timing synchronizing algorithm

Symbol timing synchronizer is a critical module of the digital receiver design of the channel sounder based on sliding correlation channel measurement. Gardner's symbol timing recovery method is used in this system [18][19]. The structure of the symbol timing synchronizer is shown in Fig. 4. All the processing of this synchronizer is done in digital domain. No interaction between analog and digital part of the system is needed. This synchronizer is capable of compensating sampling phase and frequency offset and is independent of carrier phase [20].

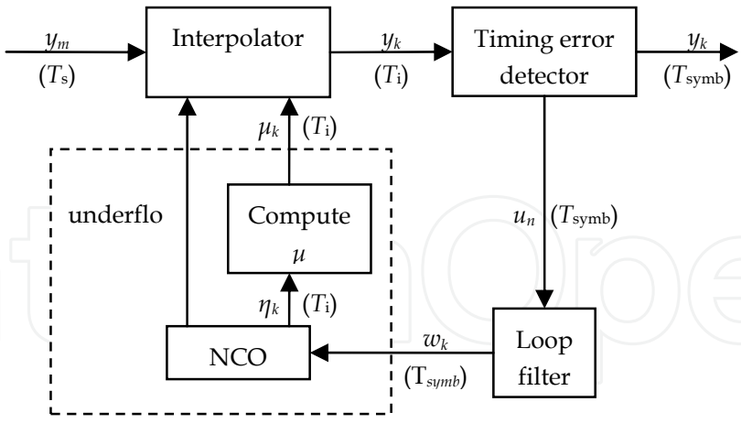

Fig. 4. Symbol timing synchronizer.

The sampled data y_m, which is filtered by matching filter, is then feed into the interpolator to compute the desired sampled strobe y_k. This is done by digital interpolation, controlled by NCO (Numerical Controlled Oscillator) and fraction interval μ_k. Ideally, the period of the NCO is $T_i = T_{symb} / K$, where K is an integer. The loop consisting of timing error detector, loop filter and NCO function just like a DPLL, where u_n, w_k and η_k represents timing error signal, NCO control word and NCO register content respectively.

In this design, the DTTL algorithm [20] is used to compute the timing error signal. This choice specifies $T_i = T_{symb} / 2$. In order to avoid up-sampling in the interpolator, T_s should be smaller than T_i. Thus, the sampling frequency f_s should be larger than two times the symbol rate R_{symb}. The interpolator performs linear interpolation, which is easy to implement. The loop filter is a proportional-plus-integral structure.

3.1.2 Hardware design

The whole measurement system hardware consists of several modules: antennas module, multi-channel AD/DA module, baseband processing FPGA board, USB access module and a computer Graphical User Interface (GUI) module. The architecture of hardware is showed in Fig. 5. The RF board is based on MAX2829, which can support MIMO operation. We choose the FFP board (IAF GmbH) as FPGA prototyping platform for baseband signal processing, RF control and interface to PC. The interface between the FFP board and the PC is an USB2.0 port. The GUI program runs on the computer for user to control the channel measurement functions and demonstrate the real time test results. Because the most effort is on the development of FPGA, here we focus on the design of baseband transceiver.

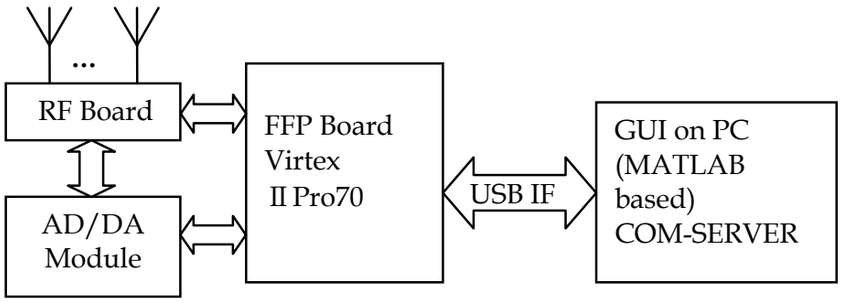

Fig. 5. Hardware architecture of the channel measurement system.

The baseband transceiver module performs the baseband signal processing of a 2x2 MIMO channel sounder. This module generates the baseband probing signal, i.e. a BPSK modulated PN sequence, and delivers the CIR extracted from the received signal to the upper-level module.

The block diagram of this module is shown in Fig. 6. The module can be divided into three parts. The first part is the transmitter, which includes signal generator and transmit multiplexer. The second part is the receiver, which includes receive buffers, signal processor, and data buffer. The last part is the control logic of the module.

The functions of the sub-modules are as follows:

- Signal generator generates the baseband probing signal, i.e. a BPSK modulated PN sequence.
- Transmit multiplexer distributes probing signal to different TX antennas.
- Receive buffers save the received signal from RX antennas.
- Receive multiplexer feed the signal stored in receive buffers into the signal processor in a sequential order.

- Signal processor performs the signal processing, i.e. filtering, symbol timing, and sliding correlation, to extract the CIR from received signal.

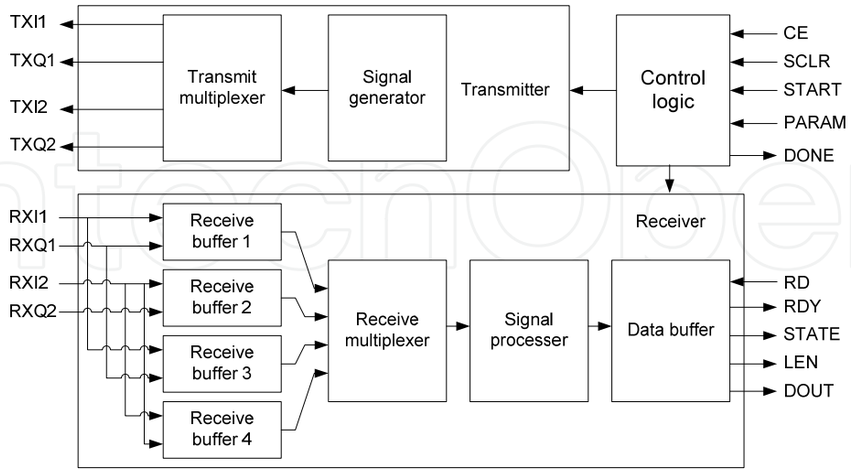

Fig. 6. Baseband transceivers.

3.1.3 GUI

To provide a user friendly human interface, we design a MATLAB based GUI. The real time data stream is accessible from the specific application software through a function call of the COM-Server from IAF. The software can provide several channel information from the original measured data. These channel information include channel impulse response, channel transfer function, delay power profile, scattering function and Doppler power spectrum. Fig. 7 is an indoor channel test result for example.

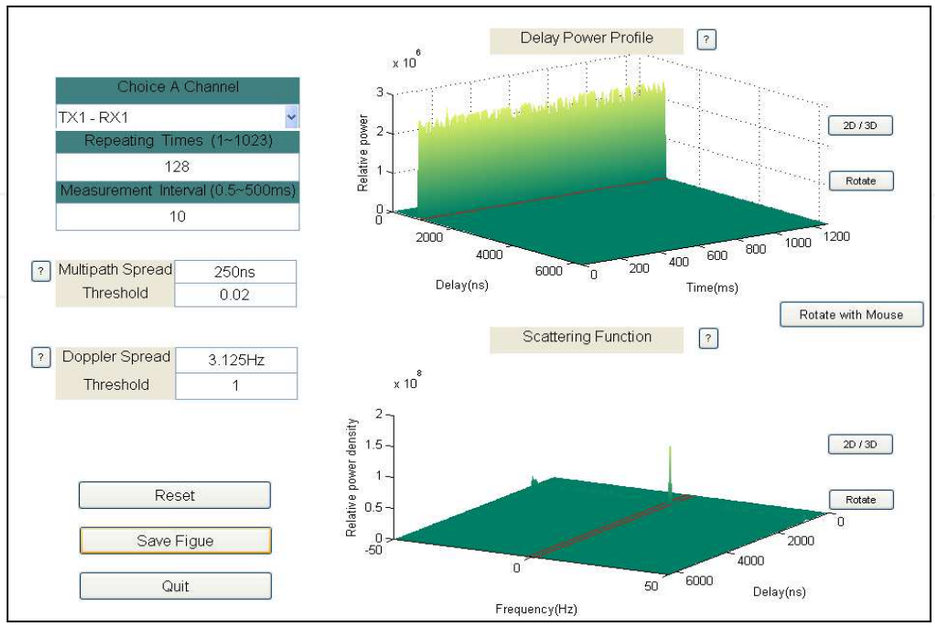

Fig. 7. Measurement result on GUI.

3.2 Channel measurement system using OFDM pilot

In the section, we present an example of OFDM-pilot-based MIMO channel measurement scheme. The measurement is conducted under LTE system. We utilize the reference signal (pilot) to carry out the 4x4 MIMO channel measurement. In this example, the measurement of channel occupied by pilots is LS algorithm, with the purpose of decreasing complexity.

One transmitter sends data according to the LTE agreement, so that each transmitted subframe consists of pilots and useful data. Receiver breaks down each subframe to obtain pilot segments and data segments, respectively. Such measurement equipment can implement the channel measurement without interrupting communications.

A cascade 1-D filtering is used for the 2-D interpolation. This cascade 1-D filtering firstly interpolates the channel in frequency domain with LMMSE interpolation, and then finishes the whole interpolation with a linear time domain interpolation.

There are several reasons why we choose a cascade of frequency LMMSE interpolation and time linear interpolation. LMMSE interpolation certainly has the best MSE performance among all the interpolation schemes. However, the complexity of LMMSE interpolation is much larger than that of linear interpolation. Thus, a tradeoff between performance and complexity has to be made. In frequency domain, LMMSE can provide a large performance increase. When achieving the same BLER or throughput performance, LMMSE interpolation can save about 2 dB SNR. On the other hand, the performance improvement in time domain by applying LMMSE interpolation is marginal, saving only 0.25 dB average. Considering the above, the usage of a cascade of frequency LMMSE interpolation and time linear interpolation is reasonable.

A block diagram of this example is showed in Fig. 8.

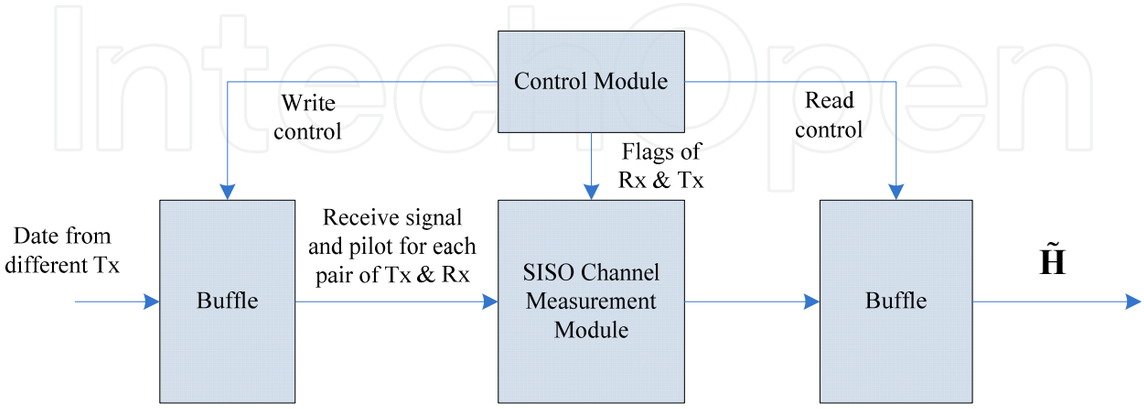

Fig. 8. A block diagram of LTE MIMO channel measurement system.

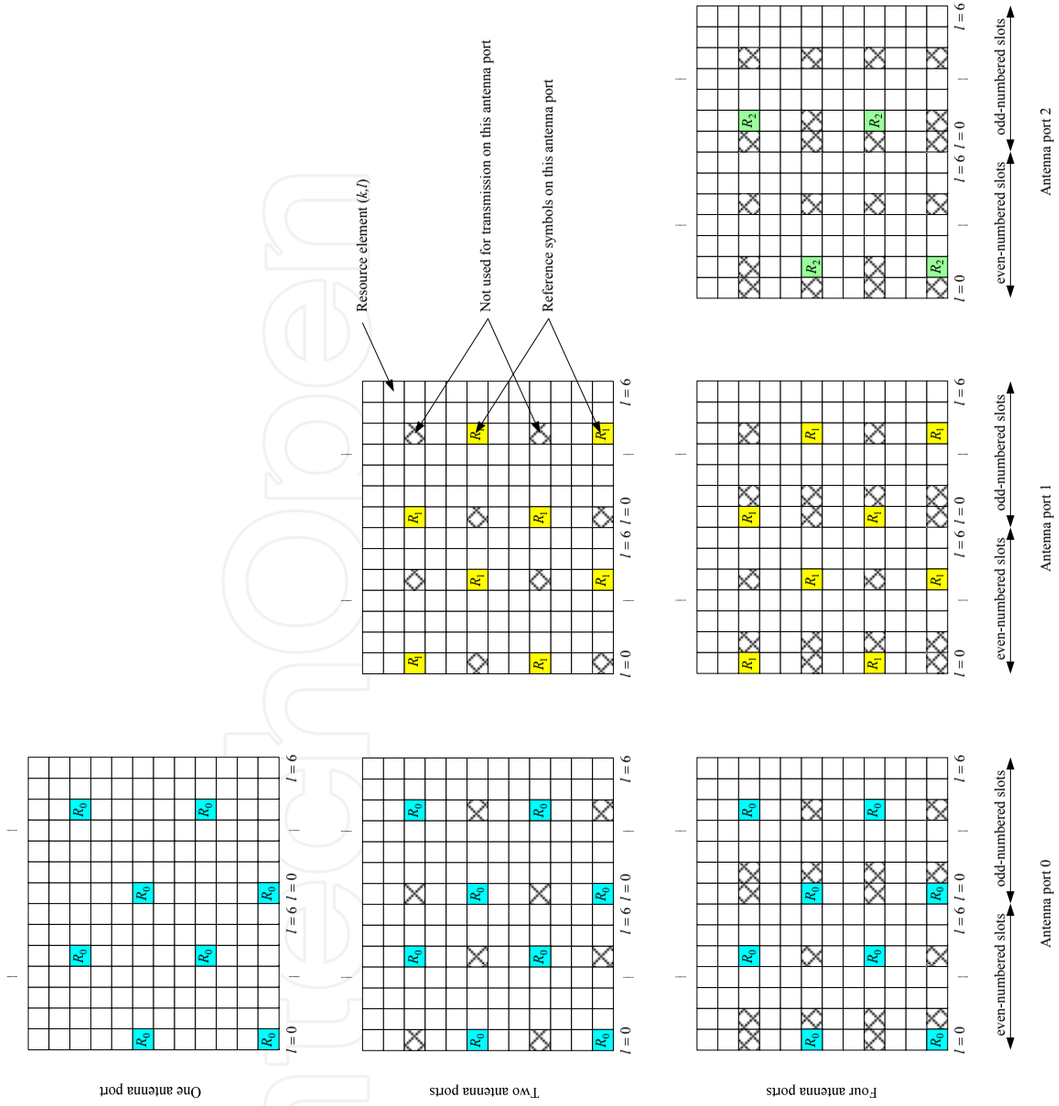

Fig. 9. Pilot pattern of LTE system [4].

3.2.1 Measurements on LTE pilots

Since LTE symbols are typical OFDM symbols, classic measurement schemes such as LS and LMMSE can be applied directly on LTE pilots. A matrix form of (12) for measured channel by LS algorithm is showed as followed:

$$\tilde{\mathrm{H}}_{\mathrm{p}}^{\mathrm{LS}}=\mathbf{X}_{\mathrm{pp}}^{-1}\mathrm{Y}_{\mathrm{p}}=\mathrm{H}_{\mathrm{p}}+\mathbf{X}_{\mathrm{pp}}^{-1}\mathrm{N}_{\mathrm{p}}=[\frac{Y_{\mathrm{p}}^{1}}{X_{\mathrm{p}}^{1}},\frac{Y_{\mathrm{p}}^{2}}{X_{\mathrm{p}}^{2}},\cdots,\frac{Y_{\mathrm{p}}^{M_{\mathrm{p}}}}{X_{\mathrm{p}}^{M_{\mathrm{p}}}}]^{T} \tag{47}$$

Since LMMSE algorithm is very vulnerable to the speed of mobile stations, the benefit brought by LMMSE will be negligible while comparing to its large processing burden. Furthermore, LS algorithm can be helpful in cancelling the effect of noise brought by LMMSE interpolation, so that the overhead of LMMSE interpolation can be reduced.

3.2.2 Design of frequency domain interpolation

Considering equation (34), there are three major challenges in realizing frequency domain LMMSE interpolation: estimating autocorrelation matrix $\bar{\mathbf{R}}_{\mathrm{h_L h_L}}$, determining Signal-to-Noise-Ratio in receiver and obtaining the inversion of matrix.

3.2.2.1 Autocorrelation matrix $\bar{\mathbf{R}}_{\mathrm{h_L h_L}}$

Since the real channels are time-varying, it is impossible to obtain the accurate autocorrelation of channels. The most widely used scheme is to estimate the approximate autocorrelation through some known channel models. It is well-known that two of the most important factors in wireless channel models are multipath spread and Doppler spread. While in the frequency domain, we mainly consider the influence of multipath spread, and propose a simple but useful construction scheme for wireless channels as followed.

The CIR of such a multipath channel is showed as followed:

$$h(\tau)=\sum_{l=0}^{N_{\mathrm{L}}-1}\mathrm{h}_{l}\delta(\tau-\tau_{l}) \tag{48}$$

Where τ_l and h_l are the delay and amplitude of the l^{th} path. N_{L} denotes the max number of taps. δ represents the impulse function.

Define $\mathrm{L}=\{0,1\cdots N_{\mathrm{L}}-1\}$. Define $\mathrm{h}\in C^{N\times 1}$, $\mathrm{h}_l=0,\forall l\in\{N_{\mathrm{L}}\cdots N-1\}$ as the multipath amplitude vector, N as subcarriers in each OFDM symbol.

Within digital baseband, we assume that the discrete delay as:

$$\tau_l=\frac{lT_{\mathrm{s}}}{N},l\in\mathrm{L} \tag{49}$$

Where is the length of an OFDM symbol.

Further assume that power σ_l^2 of independent Rayleigh-distributed tap h_l is fading exponentially with time constant τ_d:

$$\sigma_l^2 \sim e^{-\frac{l}{\tau_d}}, l \in \mathrm{L} \tag{50}$$

Then the normalized CIR autocorrelation can be expressed as:

$$\bar{\mathbf{R}}_{\mathrm{h_L h_L}} = \frac{\mathbf{R}_{\mathrm{h_L h_L}}}{\left\|\mathbf{R}_{\mathrm{h_L h_L}}\right\|} = \frac{diag(\sigma_0^2 \cdots \sigma_{N_\mathrm{L}-1}^2)}{\left\|\mathbf{R}_{\mathrm{h_L h_L}}\right\|} = \frac{diag(\sigma_0^2 \cdots \sigma_{N_\mathrm{L}-1}^2)}{\sum_i \sigma_i^2} \tag{51}$$

Base on the above derivation, we need to determine N_L and τ_d to obtain $\bar{\mathbf{R}}_{\mathrm{h_L h_L}}$. The number of available taps N_L can be same as the length of cyclic prefix (CP), with the purpose of simplification. Yet such a simplification is reasonable, since the multipath spread is less than the length of CP in most of the time. The multipath spread can be estimated with real-time scheme, so as to refine the channel model, as well as the autocorrelation $\bar{\mathbf{R}}_{\mathrm{h_L h_L}}$.

One of the possible schemes to estimate the multipath spread is provided as followed:

Step 1. Measure the channel matrix of piloted segments $\tilde{\mathrm{H}}_\mathrm{p}$ in a symbol, with LS algorithm. Take a N_p points IFFT to obtain the rough CIR $\hat{\mathrm{h}}_\mathrm{L}$, and set $N_\mathrm{L}^{\max} = N_\mathrm{p}$ as the max length of multipath spread.

Step 2. Define a parameter $\hat{h}_{\mathrm{pow}}^s$ as:

$$\hat{h}_{\mathrm{pow}}^s = \left|\hat{\mathrm{h}}_s\right|^2 \quad s = 1,2,\cdots N_\mathrm{L}^{\max} \tag{52}$$

Where $\hat{h}_{\mathrm{pow}}^s$ denotes the square of amplitude for the s-th element in $\hat{\mathrm{h}}_\mathrm{L}$.

Then obtain a decision object K_s as followed;

$$K_s = \frac{(\sum_{j=s-9}^{s} \hat{h}_{\mathrm{pow}}^j)/(2\times 10)}{(\sum_{k=s+1}^{N_\mathrm{L}^{\max}} \hat{h}_{\mathrm{pow}}^k)/(2\times(N_\mathrm{L}^{\max}-s))} \tag{53}$$

Step 3. Find a value of s by the following procedure:

Decrease the value of s from $N_\mathrm{L}^{\max} - 15$ to 1 with a step of 5. Take the first value of s that satisfies $K_s > 2.55$ as the estimate multipath spread. One can refer to [15] for the reason of choosing 2.55 as the threshold.

After determining the multipath spread, one can obtain $\bar{\mathbf{R}}_{\mathrm{h_L h_L}}$ by following previous derivation.

3.2.2.2 Signal-to-noise-ratio

SNR value may be measured or estimated in other blocks of receiver. If it is not, the following estimation scheme can be applied.

Denote $\bar{\mathbf{R}}_{\mathrm{h_L}} = \bar{\mathbf{R}}_{\mathrm{h_L h_L}}^{1/2}$, $\mathbb{F}_{\mathrm{PL}} = \mathbf{F}_{\mathrm{PL}}\bar{\mathbf{R}}_{\mathrm{h_L}}$. Do a singular value decomposition on $\mathbb{F}_{\mathrm{PL}}$, so that $\mathbb{F}_{\mathrm{PL}} = \mathbf{USV}^*$. Project estimated channel matrix $\tilde{\mathrm{H}}_\mathrm{p}$ and real channel matrix H_p as

$\mathrm{U}^{*}\tilde{\mathrm{H}}_{\mathrm{p}}$ and $\mathrm{U}^{*}\mathrm{H}_{\mathrm{p}}$. The element in the project of real channel $\mathrm{U}^{*}\mathrm{H}_{\mathrm{p}}$ tends to zero when the singular value of $\mathbb{F}_{\mathrm{PL}}$ is zero. But things are different in $\mathrm{U}^{*}\tilde{\mathrm{H}}_{\mathrm{p}}$. Since we have $\mathrm{U}^{*}\tilde{\mathrm{H}}_{\mathrm{p}} = \mathrm{U}^{*}(\mathrm{H}_{\mathrm{p}}+\mathbf{X}_{\mathrm{pp}}^{-1}\mathrm{N}_{\mathrm{p}})=\mathrm{U}^{*}\mathrm{H}_{\mathrm{p}} + \mathrm{U}^{*}\mathbf{X}_{\mathrm{pp}}^{-1}\mathrm{N}_{\mathrm{p}}$, it is clear that when the last elements of $\mathrm{U}^{*}\mathrm{H}_{\mathrm{p}}$ are zeros, the corresponding elements of $\mathrm{U}^{*}\tilde{\mathrm{H}}_{\mathrm{p}}$ reflect the impact of noise. As a result, we can estimate the noise power by these elements.

Let $\mathrm{s} = \{N_{\mathrm{p}} - N_{\mathrm{s}} \cdots N_{\mathrm{p}} - 1\}, 1 \le N_{\mathrm{s}} < N_{\mathrm{p}}$ be the range of index, N_{p} denotes the number of pilots, N_{s} represents the number of zero singular value in $\mathbb{F}_{\mathrm{PL}}$. Then the estimated noise power is $\tilde{p}_n = \frac{1}{N_{\mathrm{s}}}\left\|\mathbf{U}_{.\mathrm{s}}^{*}\tilde{\mathrm{H}}_{\mathrm{p}}\right\|_2^2$, and the corresponding signal power is $\tilde{p}_s = \frac{1}{N_{\mathrm{p}}}\left\|\tilde{\mathrm{H}}_{\mathrm{p}}\right\|_2^2 - \tilde{p}_n$. Assume that the SNR is constant within adjacent k pilots, then an average SNR can be obtain as followed:

$$\overline{SNR} = \frac{\sum_{i=1}^{k}\tilde{p}_{n_i}}{\sum_{i=1}^{k}\tilde{p}_{s_i}} \tag{54}$$

Since the last element in $\mathbf{U}_{.\mathrm{s}}^{*}\tilde{\mathrm{H}}_{\mathrm{p}}$ rarely contains signal information, it is the most suitable one for SNR estimation. Therefore, we can simplify the process by setting $N_{\mathrm{s}} = 1$.

3.2.2.3 Inversion of matrix

It is clear from equation (34) that in order to obtain the interpolation matrix $\mathbf{w}$, a N_{p} order matrix inversion operation must be conducted. The overhead will be very large. Fortunately, instead of the entire matrix, we only need several discrete $\bar{\mathbf{R}}_{\mathrm{h_L h_L}}$ matrices. Therefore, if we apply discrete average SNR in equation (34), the parameter of interpolation matrix $\mathbf{w}$ will be discrete. We can pre-design the discrete range of $\mathbf{w}$, and save it in a table. Then the real-time calculation is simplified as a looking up in a table, according to the measured $\bar{\mathbf{R}}_{\mathrm{h_L h_L}}$ and SNR.

Specifically, we can adapt a look-up table which cuts the SNR range into several intervals. Each SNR interval combines with a corresponding multipath spread $\hat{\tau}$. Each of such pairs jointly determines a pre-designed $\mathbf{w}$. With this scheme, the complexity of matrix inversion in real-time process is converted to the design of look-up table. Since the look-up table is generated off-line, real-time calculation burden for LMMSE interpolation is largely reduced.

3.2.3 Design of time domain interpolation

According to LTE standardization, each transmission time interval (TTI) is of length 1ms, which is the exact length of a subframe. Consequently, mobile stations process date in units of subframe. When time domain interpolation is conducting, there are at most four pilots in each subframe. As a result, the reference of time domain interpolation of LTE system is at most four estimated channel segments. Two of the most widely used schemes in time domain interpolation are LMMSE interpolation and linear interpolation. The detailed procedures of these two interpolations are presented in previous sections, so we only provide some simulation results to illustrate the advantages and disadvantages of each scheme.

The following simulation considers a unban macro scenario, in which the bandwidth is 10MHz, center frequency is 2GHz and noise is AWGN. Fig. 10 shows the MSE performances of both LMMSE and linear interpolations under different MS speeds.

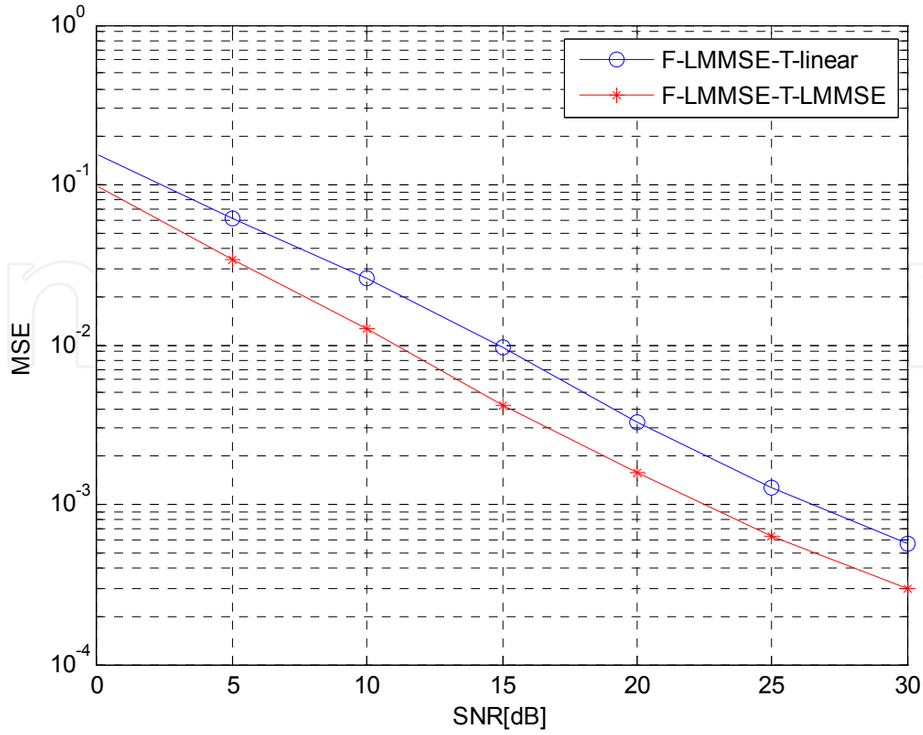

Fig. 10. (a) MSE performances of LMMSE and linear interpolations under MS speed 1m/s.

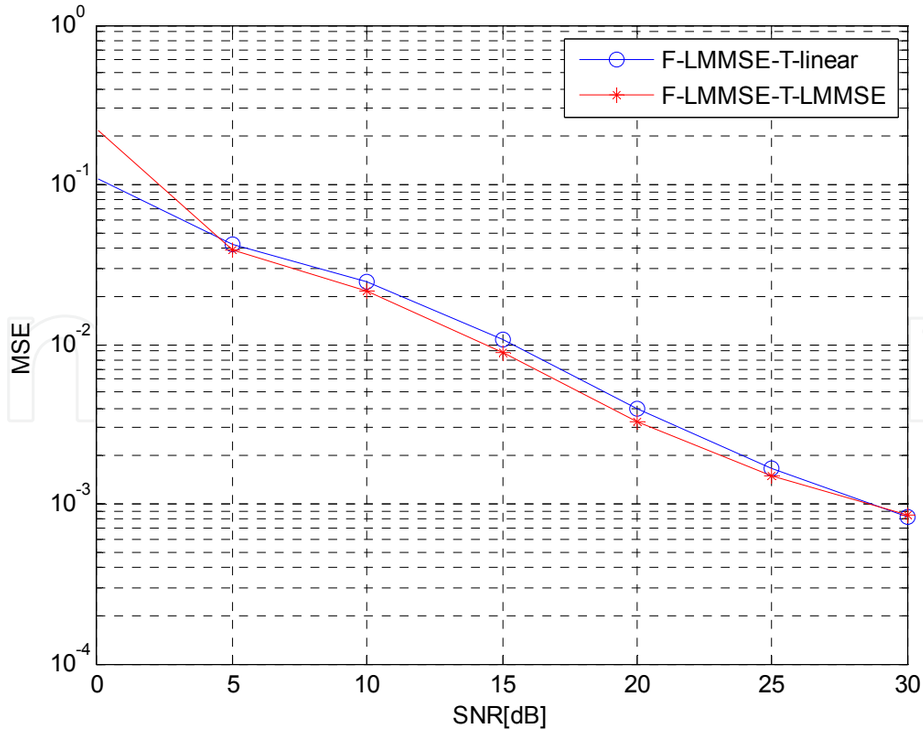

Fig. 10. (b) MSE performances of LMMSE and linear interpolations under MS speed 30m/s.

The following conclusions can be inferred from the simulation results.

When the speed of MS is small, correspondingly small Doppler spread, LMMSE interpolation can save 4 dB SNR while achieving the same MSE performance of linear interpolation. However, when the speed (as well as the Doppler spread) of MS increases to a relatively high level, performances of LMMSE and linear schemes become very close. This means that the large overhead spent on LMMSE outputs marginal gains on the performance. When the errors of Doppler spread estimations are taken into account, the MSE performance of LMMSE scheme may even be worse than that of linear interpolation. Consequently, after considering the tradeoff between performance and complexity, we propose to use a simple linear interpolation in time domain.

4. Reference

[1] I. E. Telatar, "Capacity of Multi-Antenna Gaussian channels," European Transactions on Telecommunications, vol. 10, no. 6, pp. 585–595, Nov./Dec. 1999.

[2] S. Vishwanath, N. Jindal, and A. Goldsmith, "Duality, Achievable Rates,and Sum-Rate Capacity of Gaussian MIMO Broadcast Channels," IEEE Transactions on Information Theory, vol. 49, No. 10, pp. 2658–2668, Oct. 2003.

[3] I. W. Group, "IEEE 802.11 Wireless Local Area Networks,"May 2001

[4] 3GPP TS 36.211: "Evolved Universal Terrestrial Radio Access (E-UTRA); Physical channels and modulation".

[5] M.K. Ozdemir and H. Arslan, "Channel Estimation for Wireless OFDM Systems," IEEE Communications Surveys & Tutorials, vol. 9, No. 2, pp. 18–48, 2007.

[6] Myung-Don Kim, Heon Kook Kwon, Bum Soo Park, Jae Joon Park, and Hyun Kyu Chung, "Wideband MIMO Channel Measurements in Indoor Hotspot Scenario at 3.705GHz," International Conference on Signal Processing and Communication Systems, 2010.

[7] Hui Yu, Ruikai Zhang, Xi Chen, Wentao Song, and Hailong Wang , "Design of an Indoor Channel Measurement System," International Wireless Communications and Mobile Computing Conference, 2010.

[8] Jose-Maria, Molina-García-Pardo, José-Víctor Rodríguez, and Leandro Juan-Llácer, "Polarized Indoor MIMO Channel Measurements at 2.45 GHz," IEEE Transactions on Antennas and Propagation, vol.56, no. 12, Dec., 2008.

[9] David W. Matolak, and Qian Zhang, "5 GHz Near-Ground Indoor Channel Measurements and Models," IEEE Radio and Wireless Symposium, 2009.

[10] Ye Wang, Wenjun Lu and Hongbo Zhu, "Experimental Study on Indoor Channel Model for Wireless Sensor Networks and Internet of Things," IEEE International Conference on Communication Technology, 2010.

[11] Alexandru Rusu- Casandra, Ion Marghescu and Elena Simona Lohan, "Estimators of the indoor channel for GPS-based pseudolite signal," International Symposium on Electronics and Telecommunications, 2009.

[12] L. J. Greenstein, D. G. Michelson, and V. Erceg, "Moment-Method Estimation of the Ricean K-Factor," IEEE Communications Letters, vol. 3, No. 6, pp. 175-176, 1999.

[13] Jae-Joon Park, Myung-Don Kim, and Hyun-Kyu Chung, "Characteristics of Ricean K-factor in Wideband Indoor Channels at 3.7 GHz," International Conference on Signal Processing and Communication Systems, 2010.

[14] John G. Proakis, "Digital Communications", McGraw-Hill Companies, Inc and publishing house of electronics industry, China. ,fourth edition, pp.766 , 2001.
[15] Guosong Li, "Research on channel estimation in wireless OFDM systems", Ph.D thesis, University of Electronic Science and Technology of China, 2005.
[16] IEEE P802.11n/D1.0, March 2006.
[17] MAXIM Integrated Products, Datasheet of MAX2828/2829, 19-3455, rev0, Oct. 2004
[18] F. M. Gardner, "Interpolation in digital modems – Part I: Fundamentals," IEEE Trans. Commun., vol. 41, pp. 501-507, Mar. 1993.
[19] F. M. Gardner, "Interpolation in digital modems – Part II: Implementation and performance," IEEE Trans. Commun., vol. COM-41, pp. 998-1008, Jun. 1993.
[20] F. M. Gardner, "A BPSK/QPSK timing-error detector for detector for sampled receivers," IEEE Trans. Commun., vol. COM-34, pp. 423-429, May. 1986.

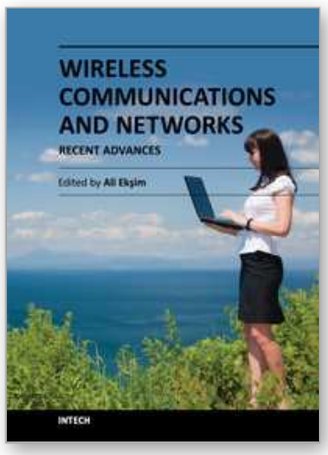

Wireless Communications and Networks - Recent Advances
Edited by Dr. Ali Eksim

ISBN 978-953-51-0189-5
Hard cover, 596 pages
Publisher InTech
Published online 14, March, 2012
Published in print edition March, 2012

This book will provide a comprehensive technical guide covering fundamentals, recent advances and open issues in wireless communications and networks to the readers. The objective of the book is to serve as a valuable reference for students, educators, scientists, faculty members, researchers, engineers and research strategists in these rapidly evolving fields and to encourage them to actively explore these broad, exciting and rapidly evolving research areas.

How to reference
In order to correctly reference this scholarly work, feel free to copy and paste the following:

Hui Yu and Xi Chen (2012). Indoor Channel Measurement for Wireless Communication, Wireless Communications and Networks - Recent Advances, Dr. Ali Eksim (Ed.), ISBN: 978-953-51-0189-5, InTech, Available from: http://www.intechopen.com/books/wireless-communications-and-networks-recent-advances/indoor-channel-measurement-for-wireless-communication

INTECH
open science | open minds

InTech Europe
University Campus STeP Ri
Slavka Krautzeka 83/A
51000 Rijeka, Croatia
Phone: +385 (51) 770 447
Fax: +385 (51) 686 166
www.intechopen.com

InTech China
Unit 405, Office Block, Hotel Equatorial Shanghai
No.65, Yan An Road (West), Shanghai, 200040, China
中国上海市延安西路65号上海国际贵都大饭店办公楼405单元
Phone: +86-21-62489820
Fax: +86-21-62489821

IntechOpen